Surv Geophys
DOI 10.1007/s10712-008-9036-0

ORIGINAL PAPER

Monitoring Flood and Discharge Variations in the Large Siberian Rivers From a Multi-Satellite Technique

F. Papa · C. Prigent · W. B. Rossow

Received: 22 October 2007 / Accepted: 9 July 2008

Abstract Using a multi-satellite method, employing passive and active microwave along with visible and infrared observations developed to estimate monthly inundation extent at global scale, this study investigates the response of river discharge to seasonal flood change in the large Siberian watersheds. The seasonal cycle and variations of inundation extent over the Ob, the Yenissey, and the Lena basins for the period 1993–2000 show different spatial and temporal behaviors due to different climate and permafrost conditions. Using in-situ discharges collected at the outlets of the three basins, we analyze and quantify the relationships between the river streamflow and the monthly satellite-derived inundation extent during the spring/summer periods. Furthermore, we analyze extreme (high/low) streamflow cases for some years and the associated inundation conditions for the three watersheds and link these cases with other climatic parameters such as the snow water equivalent, temperatures, and precipitation. The results of this study demonstrate that the monthly multi-satellite-derived inundation dataset brings a new useful tool for better understanding both the streamflow processes and the description of the snow-inundation-runoff relations in data scarce areas like the remote Arctic river basins.

Keywords Hydrology · Remote sensing · Inundation · River discharge · Snow

1 Introduction

Surface waters, which include rivers, lakes, wetlands and episodically inundated areas, continuously exchange with the oceans and the atmosphere through horizontal and vertical mass fluxes. Analysis of the flow, distribution and storage of surface waters in the global

F. Papa (✉) · W. B. Rossow
NOAA-Cooperative Remote Sensing Science and Technology Center, City College of New York, New York, USA
e-mail: fpapa@giss.nasa.gov

C. Prigent
CNRS, Laboratoire d'Etudes du Rayonnement et de la Matière en Astrophysique, Observatoire de Paris, Paris, France

water balance is thus a key issue for the understanding of the hydrological and biochemical cycles. This is particularly true for the Arctic watersheds and their hydrologic systems, which are important to global ocean and climate. Arctic Rivers represent, through their discharge, the primary driver of the Arctic Ocean freshwater budget, in turn greatly influencing the thermoaline circulation (Aagaard and Carmack 1989) and the winter sea ice cover (Dickson et al. 2001). Global warming is expected to be particularly significant in the arctic regions. One indicator of this change is that the average annual discharge of fresh water from the six largest Eurasian rivers to the Arctic Ocean has increased by 7% over the last century (Peterson et al. 2002; Yang et al. 2002).

Arctic hydrologic systems are complex and exhibit large temporal variability due to large-scale changes in atmospheric circulation (Proshutinksy et al. 1999). They are strongly influenced by the winter snow and freeze/thaw cycles (Yang et al. 2003; Frei and Robinson 1999) and studies demonstrate that the timing and magnitude of the discharge of northern rivers are strongly associated with cold season snow mass storage and subsequent melt (Rango 1997; Cao et al. 2002; Yang et al. 2003; Serreze et al. 2002). During the spring/summer period, the release of water upon melting of the winter snow accumulation may lead to extreme flooding events and thus represents the major hydrologic event of the year in the northern river basins (Cao et al. 2002; Yang et al. 2003).

Our current knowledge of the seasonal and inter-annual variability of large-scale land surface water dynamics is rather incomplete, currently relying on sparse in situ gauge measurements and partially verified hydrological models. In situ gauge measurements have helped quantifying the movement of water (discharge) in river channels but provide comparatively little information about the spatial dynamics of surface water extent in floodplains and wetlands. In addition, the availability of ground-based gauge information has dramatically decreased during the last decade (Alsdorf and Lettenmaier 2003), especially in remote areas like the Arctic watersheds (Vörösmarty et al. 2001).

Lacking spatially complete measurements of inundation/wetland locations, sizes, and water storage, hydrologic models are unable to properly partition precipitation among these several components and represent their effects on river discharge at continental-to-global scales (Alsdorf and Lettenmaier 2003). Errors on simulated river discharge can exceed 100% because inundated surfaces modulate runoff by temporarily storing and changing runoff and evaporation (Coe 2000; Alsdorf et al. 2007). Partially verified hydrological models also limit our ability to predict changes in the hydrological system in the high latitude regions under a warming climate.

Thus, reliable and timely information about the extent, spatial distribution, and temporal variation of wetlands and floods is crucial to better understand their relationship with river discharges, as well as their influence on regional hydrology and climate.

Remote sensing techniques have been very useful to cold region climate and hydrology investigations (Massom 1995; Smith 1997) as they provide a unique mean to observe large regions and are the only alternative to in situ data in remote areas. For instance, the NOAA snow cover maps are useful for hydrologic and snowmelt runoff models (Rango 1996, 1997). Using the Topex-Poseidon radar altimeter, Kouraev et al. (2005) estimated the Ob River water discharge close to the Shalekard station using the satellite-derived water levels. Recently, using a remotely sensed snow water equivalent data, Yang et al. (2007) identified a clear correspondence of river discharge to seasonal snow cover mass change. New space gravity missions, such as the GRACE mission, also offer direct measurements of the spatio-temporal variations of total terrestrial water storage (Ramillien et al. 2005; Rodell et al. 2006; Tapley et al. 2004; Frappart et al. 2006). Satellite-derived inundation extents and their dynamics over Boreal regions are also being actively investigated,

especially using active and passive microwave sensors (Mialon et al. 2005; Papa et al. 2006a, 2007). However, there have been relatively few efforts to examine the relationship between these satellite-derived inundation products with other hydrological parameters in the large Arctic watersheds.

Several studies have proven that there is a strong correlation between satellite-derived inundation area with ground measurements of river stage and discharge (Smith 1997; Frazier et al. 2003; Smith et al. 1996; Vorosmarty et al. 1996). For instance, Smith et al. (1995) used the measurements of flooded areas derived from ERS-1 SAR images to estimate the discharge of a glacial river in British Columbia and established a power-law correlation between satellite-derived water surface area and discharge.

Recently, using a multi-satellite method, including passive microwave land surface emissivities, along with active microwave, visible and near infrared observations developed to estimate global inundated area (Prigent et al. 2007; Papa et al. 2007) examined the spatial and temporal variations of the 1993–2000 monthly inundation extents in the Ob River basin and their relation at the local scale with in situ snow depth measurements and river run-off and discharge. Promising results showed a strong relationship between the inundation extent, the snowmelt date, and the snowpack depth at three in situ stations located in the southern part of the basin. Over the northern part, results show that flooding is more closely linked to the amount of water coming downstream from the southern part of the basin. Moreover, a close systematic and promising relationship was also found between the inundation extent and the in situ runoff at six locations that could be extended to larger areas.

In this paper, we use the globally applicable Remote Sensing (RS) technique we developed to quantify the spatial and temporal dynamics of wetlands and inundation at the global scale (Prigent et al. 2001a, 2007; Papa et al. 2006b) to study the streamflow hydrology in large Siberian rivers. The emphasis of this research is to examine the streamflow response to basin-wide change in inundation extent during the melting season and summer over large northern river basins. The results of this study can help improve our understanding of cold region hydrologic processes.

2 Study Area, Datasets, and Method of Analysis

2.1 The Large Siberian Watersheds

With their drainage areas ranging from 2,400,000 to 3,000,000 km^2, the Ob, Yenissey, and Lena Rivers are the three largest rivers in the Arctic. They originate in the midlatitudes and flow northward across the vast Siberian lowland towards the Arctic coast as shown on Fig. 1. For instance, the Ob River length is 3,680 km and with its major tributary, the Irtysh, it forms the longest river system in Asia. The combined discharge of these three rivers contributes to more than 45% of total freshwater flow into the Arctic Ocean (Shiklomanov et al. 2000). These three watersheds are mostly underlain by continuous and discontinuous permafrost (Zhang et al. 1999) and during the winter, a large part of these basins is covered by snow, which persists for six months or more. The latitudinal extent of these basins results in the gradual snow-melting from south to north during spring/summer seasons and leads to large flood events. During the spring/summer season, the Ob River basin is frequently described as the world's biggest swamp.

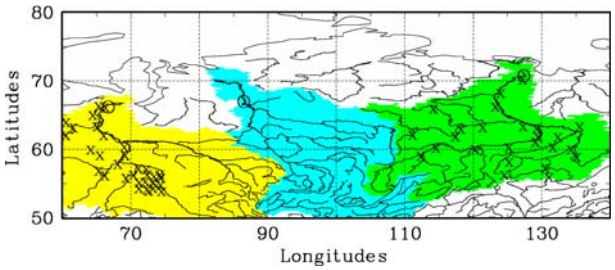

Fig. 1 The three major river basins in Siberia: the Ob (yellow), the Yenissey (blue) and the Lena (green). Also shown are the locations of the hydrologic stations at the basin outlets (O) and the locations of the in situ snow stations (X)

2.2 Datasets and Method of Analysis

The methodology developed to quantify the extent and seasonality of land inundation at global scale with a suite of satellites is described in detail in Prigent et al. (2001a, 2007). The complementary selected satellite observations used to detect and quantify inundation cover a large wavelength range:

(a) Passive microwave emissivities between 19 and 85 GHz are estimated from the Special Sensor Microwave/Imager (SSM/I) observations by removing the contributions of the atmosphere (water vapor, clouds, rain) and the modulation by the surface temperature, using ancillary data from visible and infra-red satellite observations from the International Satellite Cloud Climatology Project (ISCCP) (Rossow and Schiffer 1999) and the National Center for Environment Prediction (NCEP) reanalysis (Kalnay et al. 1996).

(b) ERS scatterometer backscatter at 5.25 GHz (5.71 cm) (active microwave): because ERS measurements are performed at different incidence angles and the repeat cycle is not short enough to provide multiple observations of the same scene with a single incidence angle during a month, a linear interpolation is applied to all incidence angles between 25 and 50 for a month and the interpolated value at 45 is used;

(c) Advanced Very High Resolution Radiometer (AVHRR) visible (0.58–0.68 μm) and near-infrared (0.73–1.1 μm) reflectances and the derived Normalized Difference Vegetation Index (NDVI) from the 8 km product generated under the joint NOAA and NASA Earth Observing System pathfinder project.

A full description of each satellite observation and the potential of merged satellite data to study wetlands and inundated surfaces can be found in Prigent et al. (2001b). The complete methodology developed to quantify water surface extent and dynamic on the global scale is illustrated in Prigent et al. (2007) and over specific regions such as India by Papa et al. (2006b).

The passive microwave emissivities are particularly sensitive to the presence of open water. The NDVI information is very important to discriminate between arid surfaces and surface waters that can have rather similar microwave emissivities. The active microwave information has a key role in the estimation of the vegetation scattering contribution within an inundated pixel. The methodology can be summarized as follows. All remote sensing data are averaged over each month on an equal area grid of 0.25 at

the equator (a pixel covers 773 km^2). An unsupervised classification of the three sources of satellite data is performed, and the pixels with satellite signatures likely related to inundations are retained. For each inundated pixel, the monthly fractional coverage by open water is obtained using the passive microwave signal and a linear mixture model with end-members calibrated with scatterometer observations to account for the effects of vegetation cover (Prigent et al. 2001a). As the microwave measurements are also sensitive to the snow cover, the snow and ice mask from the NSIDC (Armstrong and Brodzik 2005) has been used to edit the results and avoid any confusion between snow-cover and snow-free pixels. The weekly North Hemisphere snow mask given by NSIDC at 25 km interval comes from AVHRR, GOES, and other visible-band satellite data. As the melt of snow and the beginning of inundations are two events that are closely connected, we calculate the fraction of inundation when a pixel is less than 50% snow-covered.

Global monthly-mean maps of inundation extent are then created for the period 1993–2000. The technique is globally applicable without any tuning for individual environments (Prigent et al. 2007).

This dataset has been recently used for hydrologic and climatic analyses, such as the evaluation of the methane surface emission models (Bousquet et al. 2006), the validation of river flooding scheme performance in land surface models (Decharme et al. 2008), and the estimation of water volume change in the Rio Negro (Frappart et al. 2008). Recently, Papa et al. (2007) evaluated the consistency of the spatial and temporal variation of this inundation dataset over the Ob River basin using in situ snow depth and river runoff, but this was done essentially at the local scale.

Since the late 1930s, hydrological observations in the Siberian region such as the measurements of the discharges have been carried out by the Russian Hydrometeorological Service (Shiklomanov et al. 2000). Some of these observational records are now available up to 2000 (1999 for the Yenissey River) and archived at the R-Artic web site (Lammers et al. 2001; R-ArcticNet v 3.0 2003). In this analysis, we consider the monthly mean values calculated from daily discharge records collected at the basin outlet stations as shown on Fig. 1. Discharge data collected at the river mouth are particularly important as they represent freshwater input to the ocean and are often used for basin-scale water balance calculations and validation of hydrological modeling.

In this study, we examine the seasonal changes of the multi-satellite derived monthly inundation data over the large Siberian rivers for the 1993–2000 period. On the basis of this monthly dataset, we define the inundation extent climatology, the dates (at the monthly basis) of inundation appearance and their duration. We also use the monthly discharge time series collected at the outlets of the three rivers to describe the seasonal discharge variations. We analyze the monthly relation between streamflow and flood/inundation extent and examine the correlation between these two variables over the three watersheds. We finally identify extreme runoff cases and examine their correspondence with the inundation extent conditions and other climatic parameters.

In addition to streamflow and multi-satellite derived inundation extent, other datasets are thus used to help understand the response of river hydrology to inundation extent changes: (1) the basin mean monthly precipitation and temperature time series from ERA-40 reanalysis (Serreze et al. 2005; Rigor et al. 2000); (2) the monthly mean snow water equivalent (SWE) derived from SSM/I data (available for the period 1993–2000) (Armstrong and Brodzik 2001, 2002; Chang et al. 1987) and from station in situ observations from the Former Soviet Union Hydrological Snow Survey (available from 1993 to 1996 for the Ob and Lena watersheds only) (Krenke 2004).

3 Results

3.1 Monthly Inundation Extent

The seasonal cycle of the monthly basin inundation extent over the three Siberian watersheds is presented in Fig. 2. It clearly shows that the inundation characteristics are very different among the large watersheds from western and eastern Siberia. Inundation extent begins to increase around April in the Ob River basin whereas it only appears in May–June for the Yenissey and the Lena Rivers. Because of much warmer winter and spring temperatures over western Siberia (Fig. 3a), the snowmelt season starts around April in this region and gradually progresses eastward. During April, the temperatures over the Ob River basin are above 0°C and warmer by 8°C relative to the Lena watershed (Fig. 3a). It is in May that inundation appears in the Yenissey and Lena watersheds as basin mean temperatures rises above 0°C and during this period inundation extent in the Ob basin increases by more than 520%. The yearly inundation maximum extents are found to be really different among the three watersheds. The inundation maximum extent occurs in June for the Ob basin ($\sim 2 \times 10^5$ km^2) and the Lena basin ($\sim 4.7 \times 10^4$ km^2) but appears in July for the Yenissey catchment ($\sim 6.2 \times 10^4$ km^2). During May–June, similar amounts of precipitation (45–55 mm) fall in the three basins (Fig. 3b).

The seasonal cycle of the monthly and mean basin SWE from in situ data and satellite-derived estimates over the Siberian regions is presented in Fig. 4. The satellite estimates are derived from a linear algorithm using SSM/I brightness temperatures difference (Chang et al. 1987) and filtered with snow climatologies derived from NOAA weekly snow charts from 1996 to 2001 (Arctic-Rims 2003). The mean seasonal cycle derived from satellite measurements is shown in Fig. 4 for two different periods: 1993–2000 and 1993–1996, which enables a direct comparison over the same period with the SWE from in situ data. Over the Ob River basin, there is a fair agreement between the in situ and satellite SWE datasets. The satellite measurements underestimate by about 10% the in situ observations during the winter period and bigger differences are observed ($\sim 35\%$) during the melting period. Over the Lena watershed, differences are larger, especially for the typical melting season. Comparisons between SWE in situ observations and SSM/I satellite-derived estimates have been extensively discussed, with special emphasis on the limitations of the SSMI/I satellite retrievals (Chang et al. 1997; Cordisco et al. 2006; Papa et al. 2002).

However, Figs. 2 and 4 clearly indicate a response of the inundation extent to changes in the seasonal SWE in the watersheds, i.e., the inundation extent increase is associated with a decrease of basin mean SWE during the melt periods. Over the Ob watershed, both the in situ and satellite-derived SWE data show a decrease starting in April associated with warmer air temperatures (Fig. 3a) and with a decrease of basin mean SWE of $\sim 50\%$ each

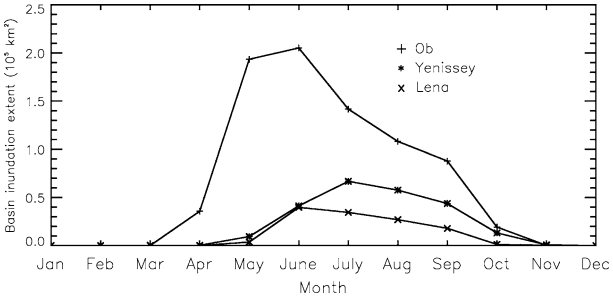

Fig. 2 1993–2000 mean monthly total inundation extent (km^2) over the three basins

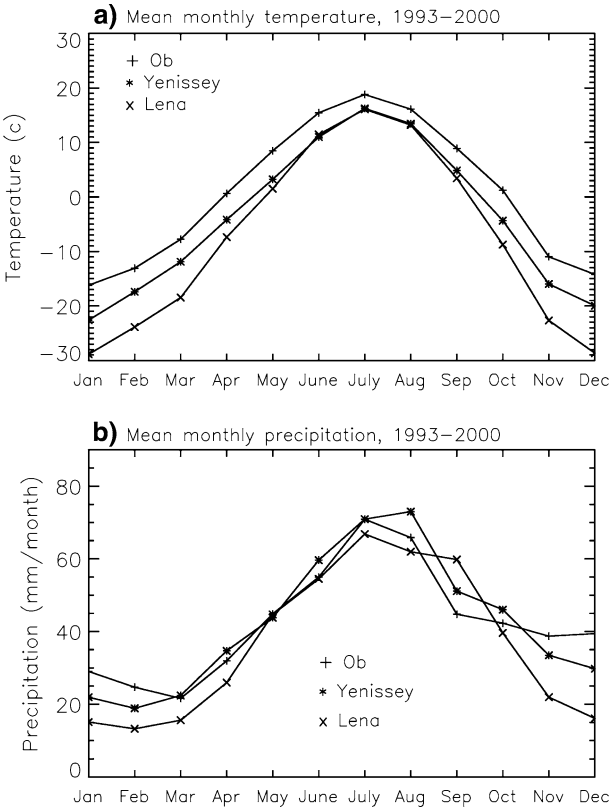

Fig. 3 1993–2000 basin mean monthly (**a**) temperature and (**b**) precipitation over the three watersheds

month until there is no more snow over the basin in June. It clearly corresponds to the appearance and increase in inundation extent over the Ob watershed as observed on Fig. 2.

Because of much colder spring temperatures, the snowmelt season starts later in the Yenissey and the Lena basins, the delay of the onset of snowmelt is 1 month over the Lena basin. The decrease in basin mean SWE from in situ observations is very high between May and June in the Lena basin ($\sim$80% in 1 month). In addition to the temperature influence, this difference in SWE decrease among the regions is likely associated with the snowpack accumulation over the winter season (a mean maximum of 112 mm of SWE over the Ob watershed is observed from in situ data compared with only 87 mm in the Lena basin). This is also in agreement with the difference in snow depth at the end of the winter derived from long-term ground observations between western and eastern Siberia (Ye et al. 1998). The decrease in SWE over the Lena basin is also well associated with the increase in inundation extents (Fig. 2).

To illustrate the evolution processes over Siberia, Fig. 5 displays the evolution of inundation extent over the three watersheds. Figure 5a shows the mean annual maximum for 1993–2000 of fractional inundation extent from satellite estimates (in %, with 100% of inundations equivalent to a 773 km^2 pixel totally flooded). Figure 5b shows the corresponding month during which the maximum inundation is reached. Figure 5c displays the difference (in months) between the first month for which inundation is detected and the

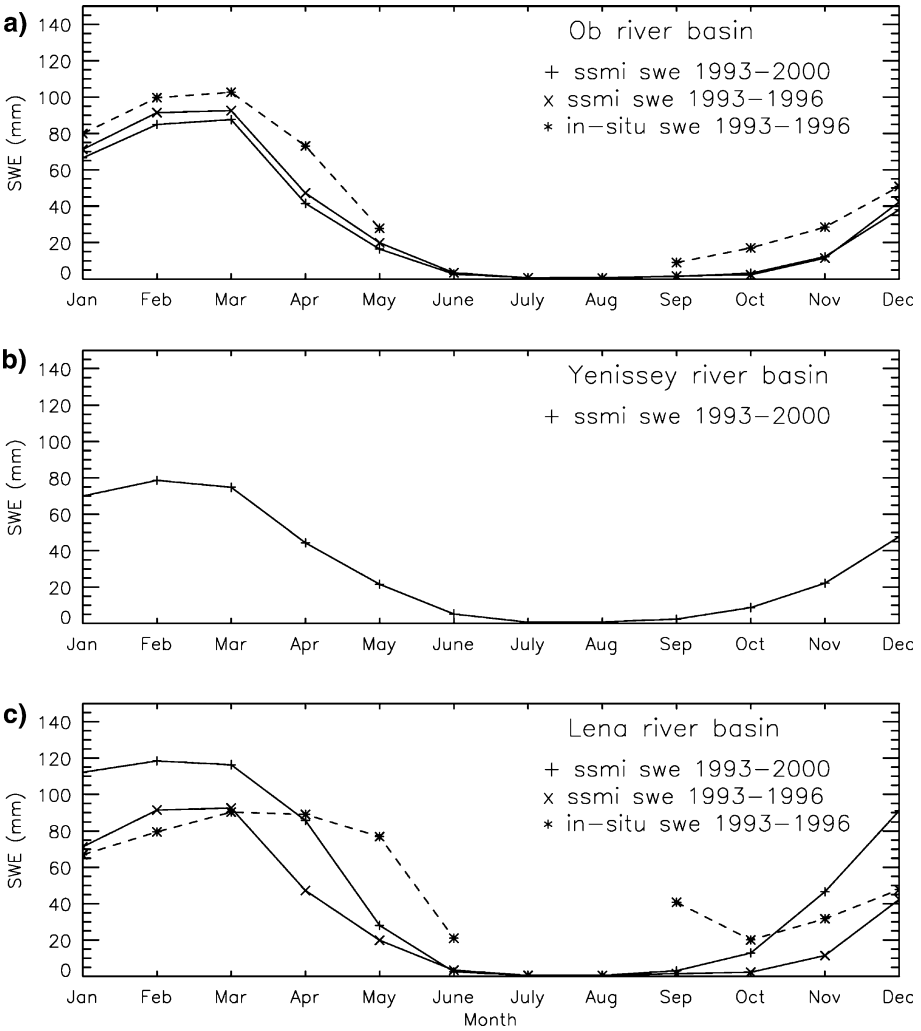

Fig. 4 Basin mean monthly Snow Water Equivalent (SWE) from satellite measurements and in situ observations (1993–1996) over the three watersheds. For the Ob and the Lena watersheds, the satellite-derived basin mean monthly SWE is given for two periods: 1993–2000 (+) and 1993–1996 (X), which enable a direct comparison with the in situ observations for the same period (1993–1996)

month for which the inundation is maximum. Figure 5a clearly shows the geographical structures of the three river systems. Over the Ob watershed, the two main rivers channels, the Ob and the Irtysh, and the associated inundation areas are well delineated. There is a strong signature with high fractional inundation extent (70–90%) in the region (60°N–64°N/65°E–75°E) where the two rivers meet. Over the Yenissey and the Lena watersheds, the main river channels and the associated flooding are also shown with fractional inundation extent at maximum ranging from 40 to 90%. It is interesting to notice that the Ob watershed exhibits much larger areas of flooding compared to the eastern Siberia watersheds ($\sim 2 \times 10^5$ km^2 for the Ob River in June; $\sim 4.7 \times 10^4$ km^2 for the Lena River in June). The Lena River is underlain by continuous permafrost (80–90%) whereas the Ob

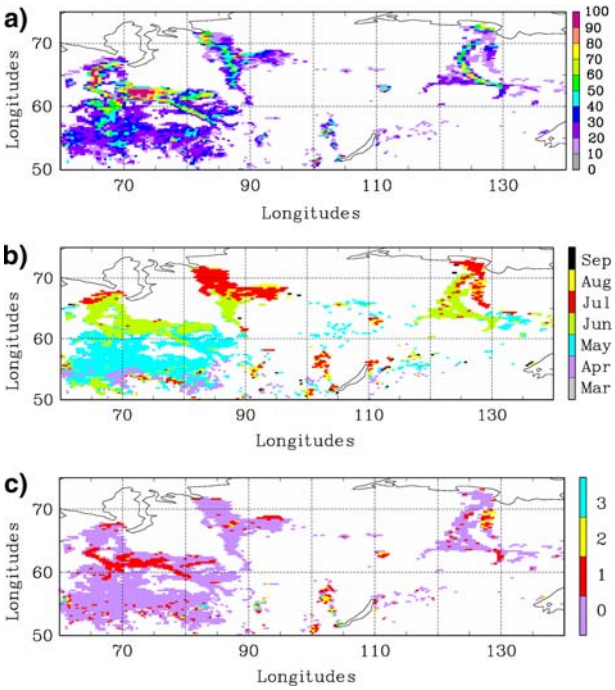

Fig. 5 Multi-satellite derived inundation characteristics over Siberia for the 1993–2000 period with a 773 km^2 spatial resolution. (**a**) the 1993–2000 mean fractional inundation at yearly maximum (%) (**b**) the average month where the fractional inundation is maximum for each year (month) (**c**) the average difference (in months) between the first month for which the inundation is detected and the month for which the inundation is maximum

basin has a permafrost coverage of about 30–40% and generally watersheds with high permafrost coverage have low surface and subsurface storage capacity (Kane 1997). These realistic structures in inundation over the three watersheds are in good agreement with the spatial features in Matthews (2000) (not shown).

Figure 5b shows the month during which maximum inundation extent occurred. Over the three watersheds, it clearly shows a propagation from south to north resulting from the latitudinal dependence of the snow melting. Over the Ob River basin, the propagation of the maximum inundation extent from south to north generally takes four months (this estimate is limited by the monthly temporal resolution of the dataset) with the maximum inundation extent occurring from April to May in the southern part of the basin (<60°N) and from May to June on the northern region (>60°N). This is in agreement with a snowmelt period around week 17–20 (April–May) in the Ob basin (Yang et al. 2003). Over the Lena catchment, the maximum inundation extent occurs during June which is in agreement with a shorter melt season over eastern Siberian regions (Yang et al. 2003).

Figure 5c displays the difference (in months) between the first month for which the inundation is detected and the months for which the inundation is maximum. Over the Yenissey and the Lena watersheds, the appearance and the maximum of flooding generally occur in the same month over the entire basin. For the Ob River basin, a noticeable difference is observed. In the lowlands and the plains of the river basin, as well as the northern part of the basin, the appearance and the maximum of inundation also occur in the

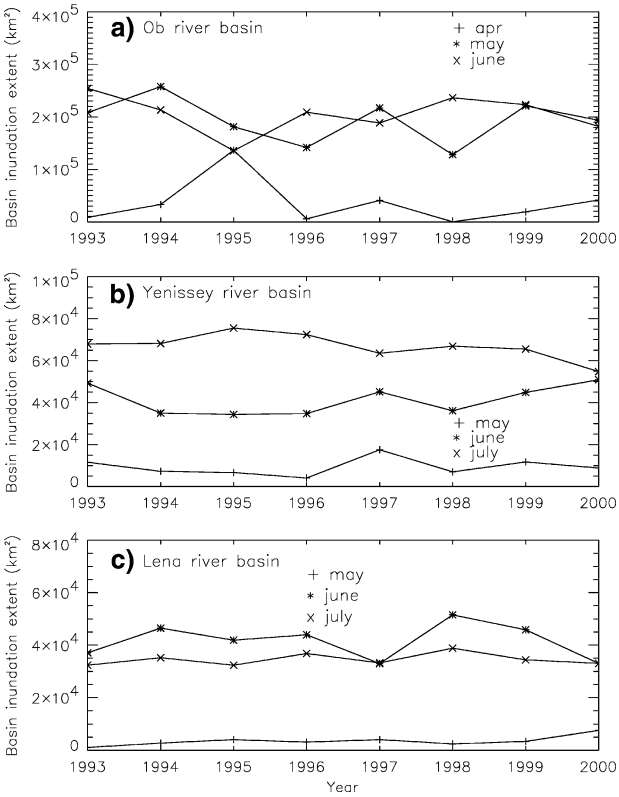

Fig. 6 Time series of monthly basin inundation extent for three different months for the period 1993–2000

same month. However, around the main two river channels, the Ob and its main tributary, the Irtysh, there is a lag of 1 month between the onset date and the date of maximum. In the plains, the flooding results in the release of water by snowmelt. These flood plains are connected through secondary channels and rivers with the large hydrographic network of the Middle Ob-Irtysh, which receives upstream and flood-plains runoff contribution. The delay in river ice breakup from south to north in this northward-flowing river yields ice jams in the northern part of the river. The water coming downstream from floodplains is stored in the main river valley, resulting in the observed widespread flooding maximum with one month lag. Finally, when the combination of the air temperature increase and the growing flood wave breaks the ice up and opens the river channel in the northern part of basin (>65°N), the first appearance of flooding and the maximum flooding occur during the same month.

The inter-annual variability of the spring inundations over the three watersheds is shown on Fig. 6. Inter-annual variations of the monthly inundation extents are large in all three watersheds. The variability of inundation extent is particularly large over the Ob watershed in April with the standard deviation being up to 120% of the mean monthly inundation extent when the southern portions of the basin are snow free and the northern parts of the basins are still covered by snow. The variability of inundation extent in May–June for the Ob is still high with standard deviation around 25% of the monthly mean. The Yenissey and the Lena rivers have a lower variability than the Ob River during the transition period of

flood start in May with a standard deviation respectively of 46 and 52% of the mean monthly inundation. In May, both eastern watersheds have a variability of inundation extent with a standard deviation of $\sim$20%; July is the month with the lowest interannual variation for both the Yenissey and the Lena with a standard deviation of 9 and 6% respectively.

In Fig. 6, we also observe that the basin inundation extents over the Yenissey watershed show a decrease in July over the 8 years. The linear regression over 1993–2000 (8 points) was found to be statistically significant with 95% confidence giving a decrease in inundation extent over the Yenissey watershed of $\sim$1,670 km^2/year i.e., $\sim$2.47% per year. A 8-year series of data is however too short to make conclusive link between spatial or temporal variations in local climate, particularly temperature, winter snow cover, or summer precipitation changes (Wang and Cho 1997).

3.2 Monthly River Discharge Regime

The seasonal cycle of monthly discharge at the basin outlets (as shown on Fig. 1) is presented in Fig. 7. They generally show a similar seasonality across Siberia, i.e., a low flow period during November to April and a high runoff season from May–June to September, with the maximum discharge occurring usually in June due to snowmelt and the associated floods. There are however noticeable differences in runoff regimes between the basins mainly due to different climate and permafrost conditions.

The river streamflow shows an early rise of discharge in April in the Ob River, however the increase in discharge for the three rivers really starts in May. The early rise of discharge in the Ob River is associated with warmer temperatures in spring producing an early melt of snow cover (Figs. 3a and 4). Discharge continues to rise in the three watersheds to reach a peak in June. In comparison to the Ob River, the rate of streamflow rise is very high in the Yenisei and Lena basins, up to 42,000 m^3/s and 65,000 m^3/s per month, respectively. As a result, the Lena River reaches peak flow in one month from the start of the snowmelt season, whereas peak flow for the Yenissey River occurs two months later and three months for the Ob River. Streamflow of the three rivers peaks at the same time (June). The magnitudes of the monthly peak flow range from 32,000 m^3/s for the Ob River to 70,000 m^3/s for the Yenisei River, and 74,000 m^3/s for the Lena basin, respectively.

Streamflow drops in July over the Yenissey and Lena watersheds, although summertime heavy rainfall events can also generate floods in the basins. The rate of discharge decreases slowlier in the Ob River than in the Lena and Yenisei basins. For instance the Ob River discharge in August is still 51% of its peak value in June, whereas it is only 20% and 32%

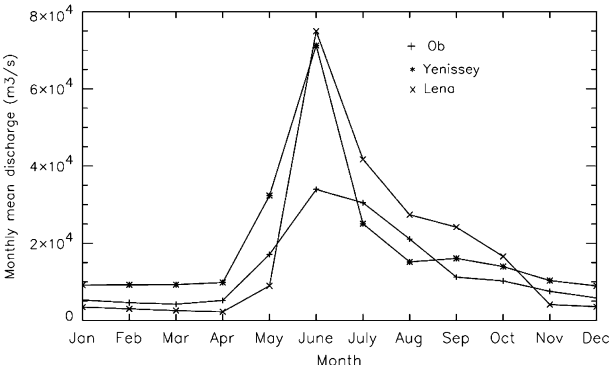

Fig. 7 Mean monthly discharge for the Ob River (1993–2000), the Yenissey River (1993–1999), and the Lena River (1993–2000)

for the Yenissey and the Lena respectively. Discharge continues to decrease to their minimum (winter) values in November.

The quicker responses of streamflow in spring/summer and faster decrease of streamflow after snowmelt in the Lena and Yenisei Rivers are related to a lower subsurface storage capacity due to a higher percentage of permafrost coverage in the central and eastern Siberian regions. The Lena River, underlain by continuous permafrost (80–90%), has a very low winter flow and a very high peak flow in June, about 40 times greater than the winter average discharge. The Yenisei River, with 60–70% permafrost, shows a lower peak runoff, reached in two months and about nine times the average discharge in winter. The Ob basin, on the other hand, with about 30–40% permafrost coverage, has the lowest peak discharge, more than a half of the other two rivers and about six times the winter average runoff.

The inter-annual variation of monthly runoff is generally small in the cold season and large over spring/summer months mainly due to the snow melt, the associated floods, and heavy rain storms.

3.3 Monthly Relation between Discharge and Inundation extent

In this section and the following ones, we will only consider the inundated areas upstream of the basin in situ gauge.

The multi-year monthly (1993–2000) means of inundation extent and river streamflow are shown together in Fig. 8. It clearly indicates a response of river runoff to seasonal inundation extent changes, i.e., an association of low streamflow with the non-presence of inundation extent during the cold season and an increase in discharge associated with an increase of inundation extent during the spring/summer period.

To quantify the relationship between variations of river runoff and basin inundation extent, we examine and compare the monthly mean streamflow with the monthly basin inundation extent for the 1993–2000 period. Figure 9 shows that the results generally confirm a very strong linkage between inundation extent and the streamflow during the spring/summer period over the large Siberian watersheds.

For the Ob River, streamflow strongly correlates with inundation extent during April, May, and June. In May, the total basin inundation extent increases sharply, up to 1.3×10^5 km^2 in 1 month. River ice breaks up around this time in the upper parts of the basin, but even if streamflow starts to increase, it does not show a clear response at the basin outlet due to ice jams in the river valleys. In June, river channels open up in the northern parts of the watershed and discharge at the basin mouth reaches its maximum. This is reflected by a strong positive correlation between runoff and inundation extent. In July, both discharge and inundation extent decrease but remain still high due to the high surface storage capacity of the watershed and less permafrost in the Ob River basin.

The Yenissey and the Lena have a slightly different behavior and both show similar processes with a strong monthly relation in June. The early melt period of snow is associated with a sharp increase in both the basin total inundation extent and the discharge at the outlet of the basin (May–June for the Yenissey, June for the Lena). Both inundation extent and discharge sharply decrease from July with values returning to 20–40% of their maximum in 1 month.

Figure 10 clearly illustrates the similarities and differences in the mean monthly cycle of processes that link the inundation extent and the response in discharge for the three watersheds. For the Ob, the Yenissey and the Lena river basins, one can observe a strong

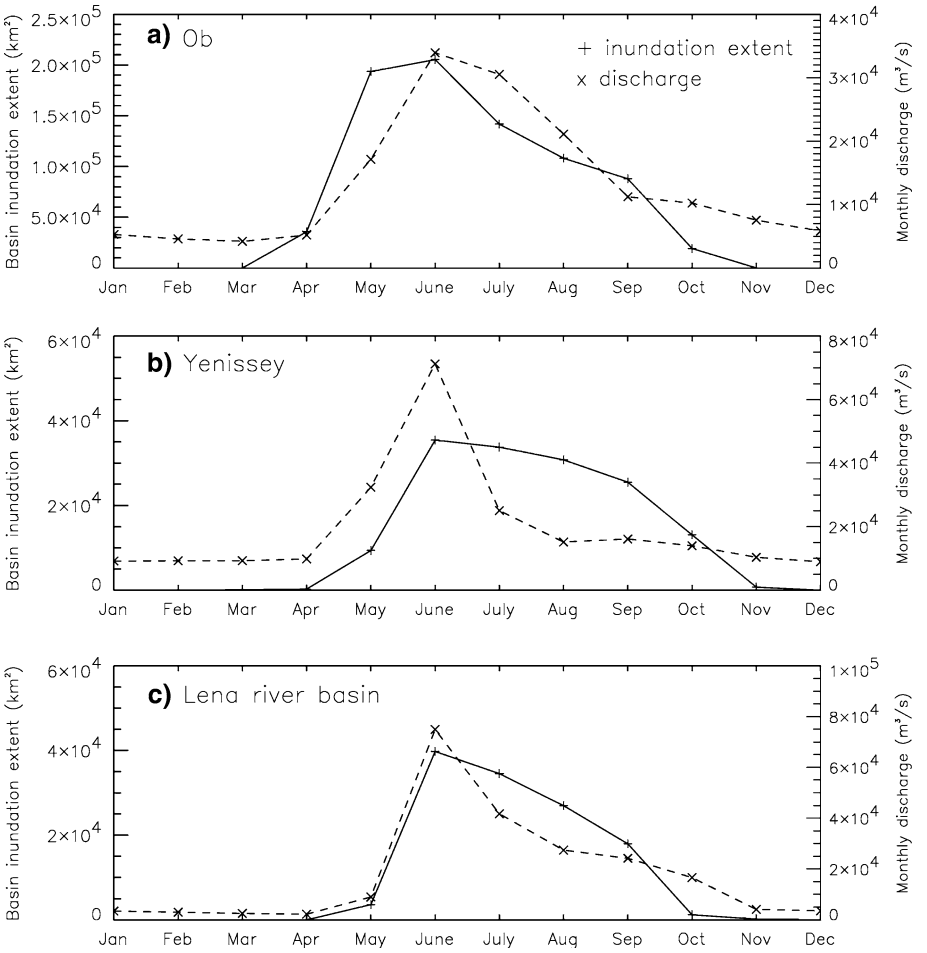

Fig. 8 Comparison of seasonal cycles between monthly inundation extent and streamflow over the three rivers

hysteresis behavior in the discharge-flood area curves. For the Ob river basin, the mean rising period in inundation and river discharge is from April to June (to be related to Figs. 8 and 9) with a large increase of both inundation and discharge as the snow melting season starts. With both the inundation and the discharge at maximum in June, the inundation areas show a sharp decrease while the river discharge remains high in July. This hysteresis between water extent and discharge for the Ob River could indicate widespread shallow flooding in the river basin, especially in the southern part of the Ob watershed (see Fig. 5). These shallow inundation areas rapidly dry out after the end of the snow melt season, while large water masses remain stored in the main floodplains and river channels in the northern regions which continue to receive water from the entire watershed. The Yenissey and the Lena basins show a different hysteresis behaviour than the Ob basin with a sharp rising period both in inundation and discharge from May to June and a sharp decrease in the July–August discharge while flood extent only slowly retracts. In this case, the connection between river channel and surrounding floodplains is certainly interrupted

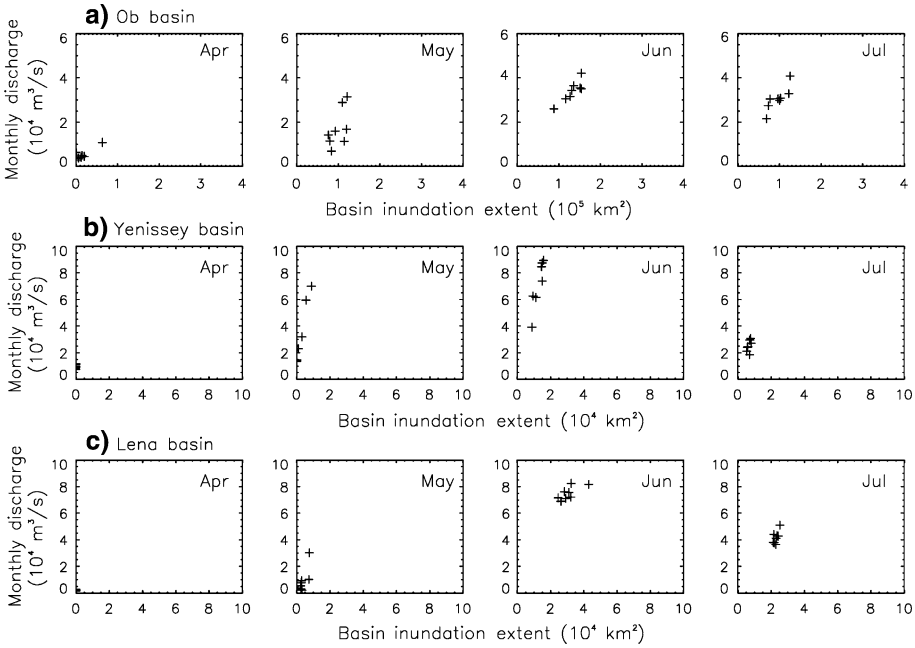

Fig. 9 Scatterplots of monthly discharge versus monthly basin inundation extent for selected months, 1993–2000

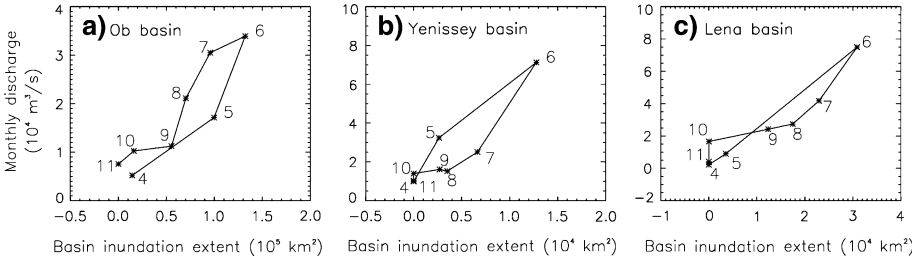

Fig. 10 The mean monthly cycle of discharge responses to inundation extent for the three watersheds. The numbers in the figures represents the months of the year

during the flood recession and could explain the change in the discharge-flood area relationship. Water that is ponding in the lowlands and that is disconnected from the river channel only slowly disappears through evaporation and percolation during the summer period.

A relation between discharge and inundation extent was derived by a regression analysis for the warm season. It shows that the correlation between runoff and inundation extent variation is the strongest during the flood rising period for the Ob River and the Yenissey watersheds. The Lena basin shows strong correlation during both flood rising and falling period.

For the Ob watershed, we separated the basin into two parts, located north and south of latitude 60°N. This separation is justified by the south to north gradual mean appearance of inundation with a limit around the latitude 60°N illustrated in Fig. 5c and the cycle of

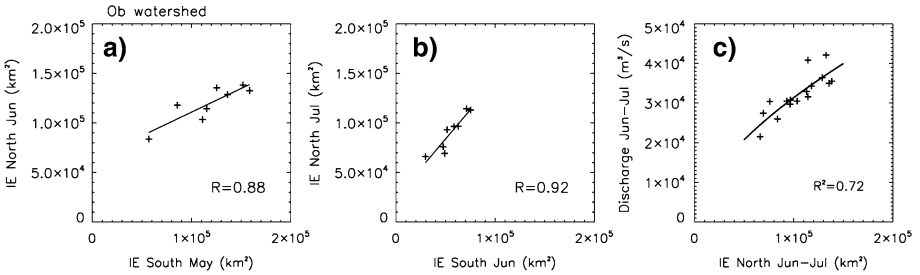

Fig. 11 Ob River basin: (**a**) and (**b**) regression relation between the inundation extent (*IE*) in the southern part of the basin and the inundation extent in the northern part with one-month difference; (**c**) regression relation between monthly discharge and basin inundation extent (northern part) during flood rising period 1993–2000

relationship between the discharge and the inundation extent shown in Fig. 10. Figure 11a shows a significant relation for the Ob basin between the inundation extent for the northern part of the basin in June and the inundation extent for the southern part of the basin in May ($y = 0.477x + 63218.5$). A close relationship is also found between the northern and the southern parts between June and July ($y = 1.182x + 24754.0$, Fig. 11b). The figure clearly indicates that in the case of a large hydrographic network with high capacity storage, such as the Ob River basin, downstream flooding is fed by the large upstream basin and that the magnitude may be predicted (a month in advance regarding the monthly resolution of this dataset) by knowing the amount of water draining from the upstream basin.

The strongest relationship between the inundation extent of the northern part of the basin and the discharge for the Ob river basin is then observed during the flood rising period in June and July (Fig. 11c) with inundation and discharge increasing together and based on a power-law model:

$$Q = aIE^b \tag{1}$$

where *IE* is the Inundation Extent, Q is the discharge, and a and b are two empirical parameters determined by a linearization of Eq. 1. For the Ob River, $a = 32.786$ and $b = 0.596$. The regression derived for the Ob river explains 72% of the discharge variability and is statistically significant at 99% confidence. The relationship between the inundation surfaces and the discharge for the Yenissey watershed (Fig. 12, $a = 364.392$; $b = 0.561$) are also highly significant during the rising period explaining 94% of the

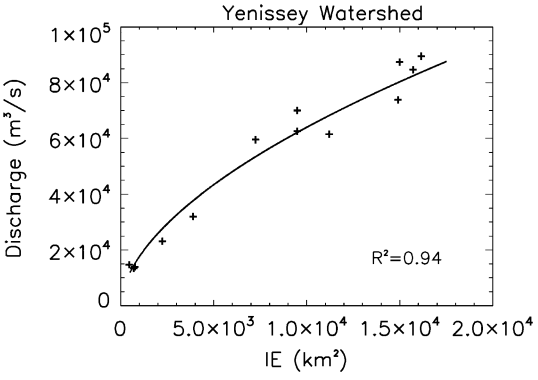

Fig. 12 Yenissey River basin: regression relation between monthly discharge and basin inundation extent during flood rising period 1993–1999

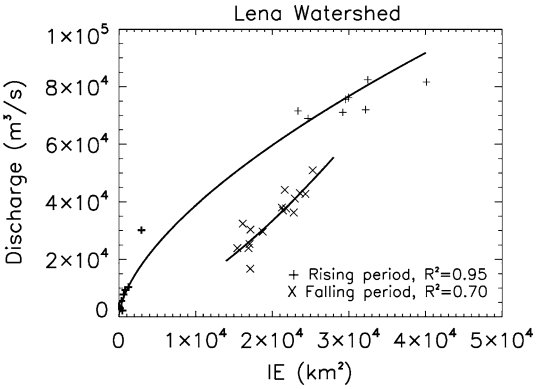

Fig. 13 Lena River basin: regression relation between monthly discharge and basin inundation extent during flood rising and flood falling periods 1993–2000

variability of the discharge with 99% confidence. For the Ob and the Yenissey rivers, no simple analytical relationship was found during the flood recession period. However, the dependence between discharge and inundation extent is very strong in the Lena River (Fig. 13) during the rising period ($a = 125.616$; $b = 0.6222$) and the falling period ($a = 0.011$; $b = 1.50$) with the regression explaining 95–70% of the discharge variability at 99% confidence.

With a longer inundation dataset that might confirm the present results, the regressions quantified here will be very useful, as they suggest a practical procedure to use the inundation dataset information to improve runoff/discharge modeling and prediction over the large Siberian watersheds.

3.4 Extreme Discharge and Associated Inundation Condition

Discharge data show a yearly peak that varies widely in magnitude and time, year to year. To understand this variability, it is necessary to examine inundation extent conditions associated with extreme runoff cases and their relationships with other climate parameters. The years of highest and lowest peak flows were selected for each watershed from the period 1993–2000.

Discharge in spring 1999 was much higher in the Ob River basin than the normal maximum (Fig. 14a, 1994 was also higher but we decide to show 1999) and the peak was reached at the normal observed date in June. The inundation extent was lower in April than the normal extent, but larger in May, suggesting a late snowmelt season as April basin mean temperatures were $\sim$2°C lower than normal. The amount of water available from the higher flood extent in May, associated with higher precipitation in 1999 (+6 mm than normal), then drained into the northern part of the basin in one month inducing larger June inundation extent and explaining the higher peak discharge in June. On the other hand, the peak flow was lower in 1995 (Fig. 14b) and the maximum was reached in May instead of June. The inundation extent was also smaller than normal in May. This case was associated with an early snowmelt season due to a warmer spring (temperatures in April were $\sim$4°C above normal) and with a lower winter snow accumulation. The basin mean SWE in 1995 was 82 mm in March, which is 6.5 mm lower than the 1993–2000 averaged SSMI-derived SWE of 88.5 mm. Moreover, it was 11 mm in April, which is 28 mm lower than the 1993–2000 average of 39 mm.

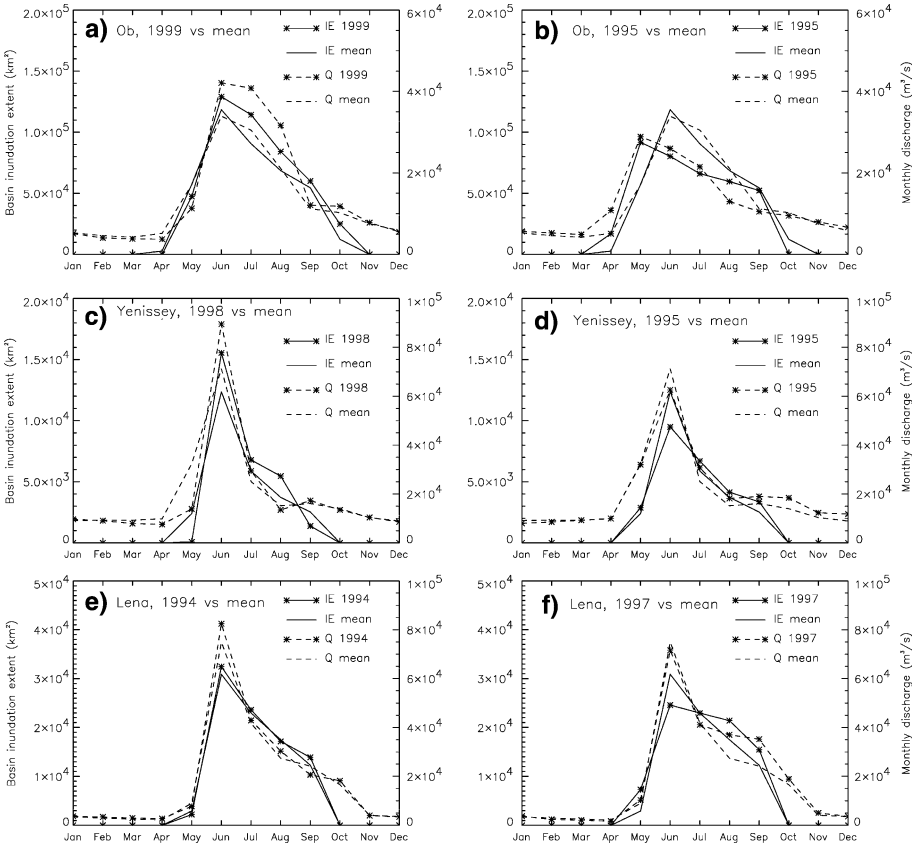

Fig. 14 Comparison of extreme (high on the left, low on the right) discharge and associated inundation extent conditions over the three watersheds

The Yenissei basin had a large peak flow associated with larger flood extent in 1998 (Fig. 14c). The discharge in June was 27% higher than the normal discharge and the inundation extent for the same month was 25% larger than its mean over 1993–1999. In May, both the discharge and the inundation extent were smaller than normal, indicating a late melt season, but this was not confirmed when looking at the basin mean temperatures or the mean basin SWE. However, in June, the basin-mean precipitation was 7 mm larger than the normal 59 mm. The small inundation extent and the associated small peak discharge in 1995 (Fig. 14d) have the same explanation as for the Ob River in 1995 with an early snowmelt season when temperatures in April–May were 3–5°C above normal.

Discharge and inundation extent in spring of 1994 were higher in the Lena basin (Fig. 14e), due a larger snow accumulation during the winter season with the mean basin SWE higher by 12 mm than the normal before the melting season. On the other hand, 1997 had smaller discharge/inundation during spring in the Lena catchment (Fig. 14f). This can be explained by the smaller snow accumulation during the winter season with the mean basin SWE smaller by 12 mm than the normal before the melting season. However during 1997 summer season, both the discharge and the inundation extent decrease more slowly than the normal until September, mainly due to heavy rain during July–August: precipitation was larger by 20–30 mm than normal in the northern part of the basin.

4 Conclusion

In this study we investigate the response of river discharge to changes in seasonal inundation extent over the large Siberian watersheds. Using a multi-satellite method that provides monthly inundation extent at global scale, we defined the seasonal cycle and variations of inundation extent over the Ob, the Yenissey, and the Lena basins for the 1993–2000 period. It shows that the three rivers have inundations with different spatial and temporal behaviors from western to eastern Siberia. We identified a clear correspondence between the yearly inundation beginning and the depletion in the winter snow cover/snow water equivalent due to the temperature increase during the spring season. Using in situ discharge collected at the outlets of the three basins, we established the relationships between the river streamflow and the change in seasonal inundation extent, i.e., an increase in discharge is associated with an increase in inundation during the spring/summer periods of 1993–2000. The results and regression analysis revealed a statistically significant relationship between the streamflow and the inundation extent during the spring/summer season over the large Siberian watersheds. Furthermore, we analyzed extreme (high/low) streamflow cases for some years and the associated inundation conditions for the three watersheds and link these cases with other climatic parameters such as the snow water equivalents, the temperatures, and precipitations.

The results of this study demonstrate that the monthly satellite-derived inundation dataset is a new useful tool to better understand streamflow processes in the Arctic regions. Monitoring the flood variability in the northern river basin is fundamental to estimate the variability of freshwater flux to the Artic Ocean. The strong relationship established in this study between the inundation extent and the streamflow could help predict year-to-year discharge variations in large Siberian watersheds and represents a useful step to improve the description of the snow-inundation-runoff relations in hydrological models over boreal river basins.

Further work has to be done to investigate the relationships found in this paper by extending the dataset to a longer time period and possibly with a better temporal resolution (weekly or daily). With the inundation dataset soon available until 2005, a longer dataset will help better characterize the variability factors and refine the regression analysis between river discharge and inundation area. The relationship between winter snow accumulation and spring flood needs also further investigation. Papa et al. (2007) already showed a good agreement at the local scale between in situ snow depth measurements and inundation extent variations during the snow melting period: it should be extended to the basin scale using satellite-derived SWE from SSM/I or GRACE measurements. This will greatly improve our understanding of the snow-flood-discharge processes in the Siberian Rivers. Other large river basins in the Artic regions, like the McKenzie, should be also considered.

This global data set of inundation variations shows also high potentials to improve our understanding of the hydrological process in temperate and tropical river basins. Similar analysis of the precipitation-flood-discharge relationships and processes in the Amazon and the Congo basins are already underway. For instance, for the Amazon basin, the annual variations of rainfall lead the variations of the inundation by 2 months revealing large water transport times through the river network. Such results can help improving and evaluating model representation of global surface water dynamics (Decharme et al. 2008).

Finally, using the global satellite-derived inundation dataset, several studies are now under investigation. In particular, combination with other data sets in order to derive crucial parameters, such as surface water storage, shows high potentials. Frappart et al. (2008) computed maps of monthly surface water volume change over eight successive

years (1993–2000) by combining the inundation dataset with altimetric observations and in situ data over the basin of the Rio Negro in the Amazon basin. The results showed a good agreement with water volume change inferred from the GRACE satellite for an average annual cycle, with precipitation and river discharge. Papa et al. (2008) showed that this technique could be extended to other large mid-latitudes and tropical watersheds like the entire Amazon, the Mississippi, the Niger and the Ganges river basins with an ultimate goal to derive surface water volume change at global scale. Surface water volume change, together with GRACE-derived total water storage, precipitation, and river discharge, will help analyze the variations of the water balance equation components at basin-continental scale and improve model representation of global surface water dynamics.

Acknowledgments We are grateful to the Arctic-RIMS team and people from the University of New Hampshire who are kindly providing data sets (river discharge, air temperature, precipitation, SSM/I-derived snow water equivalent) over the Arctic regions. We also thank the NSIDC for providing in situ snow water equivalent from the Former Soviet Union hydrological snow surveys. This research is supported by a NASA's NEWS Grant NNDX7AO90E managed by Dr. Jared K. Entin.

References

Aagaard K, Carmack EC (1989) The role of sea ice and other fresh water in the Arctic circulation. J Geophys Res 94(C10):14485–14498. doi:10.1029/JC094iC10p14485

Alsdorf DE, Lettenmaier DP (2003) Tracking fresh water from space. Science 301:1492–1494. doi:10.1126/science.1089802

Alsdorf DE, Rodrìguez E, Lettenmaier DP (2007) Measuring surface water from space. Rev Geophys 45:RG2002. doi:10.1029/2006RG000197

Arctic-RIMS (2007) A regional, integrated, hydrological monitoring system for the Pan-Arctic land mass. http://rims.unh.edu/

Armstrong RL, Brodzik MJ (2001) Recent Northern Hemisphere snow extent: a comparison of data derived from visible and microwave sensors. Geophys Res Lett 28(19):3673–3676. doi:10.1029/2000GL012556

Armstrong RL, Brodzik MJ (2002) Hemispheric-scale comparison and evaluation of passive microwave snow algorithms. Ann Glaciol 34:38–44. doi:10.3189/172756402781817428

Armstrong RL, Brodzik MJ (2005) Northern Hemisphere EASE-Grid weekly snow cover and sea ice extent version 3. National Snow and Ice Data Center, Boulder

Bousquet P, Ciais P, Miller JB, Dlugokencky EJ, Hauglustaine DA, Prigent C et al (2006) Contribution of anthropogenic and natural sources to atmospheric methane variability. Nature 443:439–443. doi:10.1038/nature05132

Cao Z, Wang M, Proctor B, Strong G, Stewart R, Ritchie H et al (2002) On the physical process associated with water budget and discharge over the Mackenzie basin during 1994/95 water year. Atmos Ocean 40(2):125–143. doi:10.3137/ao.400204

Chang ATC (1997) Snow parameters derived from microwave measurements during the BOREAS winter field campaign. J Geophys Res 102(24):29663–29671. doi:10.1029/96JD03327

Chang ATC, Foster JL, Hall DK (1987) Nimbus-07 SMMR derived global snow cover parameters. Ann Glaciol 9:39–44

Coe MT (2000) Modeling terrestrial hydrological systems at the continental scale: Testing the accuracy of an atmospheric GCM. J Clim 13:686–704. doi:10.1175/1520-0442(2000)013<0686:MTHSAT>2.0.CO;2

Cordisco E, Prigent C, Aires F (2006) Snow characterization at a global scale with passive microwave satellite observations. J Geophys Res 111:D19102. doi:10.1029/2005JD006773

Decharme B, Douville H, Prigent C, Papa F, Aires F (2008) A new river flooding scheme for global climate applications: off-line evaluation over South America. J Geophys Res 113:D11110. doi:10.1029/2007JD009376

Dickson B, Yashayaev I, Meincke J, Turrell B, Dye S, Holfort J (2001) Rapid freshening of the deep North Atlantic Ocean over the past four decades. Nature 416:832–837. doi:10.1038/416832a

Frappart F, Ramillien G, Biancamaria S, Mognard NM, Cazenave A (2006) Evolution of high-latitude snow mass derived from the GRACE gravimetry mission (2002–2004). Geophys Res Lett 33:L02501. doi:10.1029/2005GL024778

Frappart F, Papa F, Famiglietti JS, Prigent C, Rossow WB, Seyler F (2008) Interannual variations of river water storage from a multiple satellite approach: a case study for the Rio Negro River basin. J Geophys Res. doi:10.1029/2007JD009438

Frazier P, Page K, Louis J, Briggs S, Robertson AI (2003) Relating wetland inundation to river flow using Landsat TM data. Int J Remote Sens 24(19):3755–3770. doi:10.1080/0143116021000023916

Frei A, Robinson DA (1999) Northern Hemisphere snow extent: regional variability 1972–1994. Int J Climatol 19(14):1535–1560. doi:10.1002/(SICI)1097-0088(19991130)19:14<1535::AID-JOC438>3.0.CO;2-J

Kalnay E, Kanamitsu M, Kistler R et al (1996) The NCEP/NCAR 40-year reanalysis project. Bull Am Meteorol Soc 77:437–470. doi:10.1175/1520-0477(1996)077<0437:TNYRP>2.0.CO;2

Kane DL (1997) The impact of Arctic hydrologic perturbations on Arctic ecosystems induced by climate change. In: Oechel WC (ed) Global change and Arctic terrestrial ecosystems. Ecol Stud 124:63–81. Springer-Verlag, New York

Kouraev AV, Zakharova EA, Samain O, Mognard NM, Cazennave A (2005) Ob' River discharge from Topex-Poseidon satellite altimetry (1992–2002). Remote Sens Environ 93:238–245. doi:10.1016/j.rse.2004.07.007

Krenke A (2004) Former Soviet Union hydrological snow surveys, 1966–1996. National Snow and Ice Data Center/World Data Center for Glaciology, Boulder

Lammers R, Shiklomanov A, Vorosmarty C, Fekete B, Peterson B (2001) Assessment of contemporary Arctic river runoff based on observational discharge records. J Geophys Res 106(D4):3321–3334. doi:10.1029/2000JD900444

Massom R (1995) Satellite remote sensing of polar snow and ice: present status and future directions. Polar Res 31(177):99–114

Matthews E (2000) Wetlands. In: Khalil MAK (ed) Atmospheric methane: its role in the global environment. Springer-Verlag, New York, pp 202–233

Mialon A, Royer A, Fily M (2005) Wetland seasonal dynamics and interannual variability over northern high latitudes derived from microwave satellite data. J Geophys Res 110:D17102. doi:10.1029/2004JD005697

Papa F, Legresy B, Mognard NM, Josberger EG, Remy F (2002) Estimating terrestrial snow depth with the Topex-Poseidon altimeter and radiometer. IEEE Trans Geosci Remote Sens 40:2162–2169. doi:10.1109/TGRS.2002.802463

Papa F, Prigent C, Rossow WB, Legresy B, Remy F (2006a) Inundated wetland dynamics over boreal regions from remote sensing: the use of Topex-Poseidon dual-frequency radar altimeter observations. Int J Remote Sens 27:4847–4866. doi:10.1080/01431160600675887

Papa F, Prigent C, Durand F, Rossow WB (2006b) Wetland dynamics using a suite of satellite observations: a case study of application and evaluation for the Indian Subcontinent. Geophys Res Lett 33:L08401. doi:10.1029/2006GL025767

Papa F, Prigent C, Rossow WB (2007) Ob' River flood inundations from satellite observations: a relationship with winter snow parameters and river runoff. J Geophys Res 2007JD008451, doi:10.1029/2007JD008451

Papa F, Güntner A, Frappart F, Prigent C, Rossow WB (2008) Variations of surface water extent and water storage in large river basins: a comparison of different global data sources. Geophys Res Lett 35:L11401. doi:10.1029/2008GL033857

Peterson BJ, Holmes RM, McClelland JW, Vorosmarty CJ, Lammers RB, Shiklomanov AI (2002) Increasing river discharge to the Artic Ocean. Science 298:2171–2173. doi:10.1126/science.1077445

Prigent C, Matthews E, Aires F, Rossow WB (2001a) Remote sensing of global wetland dynamics with multiple satellite data sets. Geophys Res Lett 28:4631–4634. doi:10.1029/2001GL013263

Prigent C, Aires F, Rossow WB, Matthews E (2001b) Joint characterization of vegetation by satellite observations from visible to microwave wavelength: a sensitivity analysis. J Geophys Res 106:20665–20685. doi:10.1029/2000JD900801

Prigent C, Papa F, Aires F, Rossow WB, Matthews E (2007) Global inundation dynamics inferred from multiple satellite observations, 1993–2000. J Geophys Res 112:D12107. doi:10.1029/2006JD007847

Proshutinksy A, Polyakov I, Johnson M (1999) Climate states and variability of Arctic ice and water dynamics during 1946–1997. Polar Res 18(2):135–142. doi:10.1111/j.1751-8369.1999.tb00285.x

Ramillien G, Frappart F, Cazenave A, Güntner A (2005) Time variations of the land water storage from an inversion of 2 years of GRACE geoids. Earth Planet Sci Lett 235:283–301. doi:10.1016/j.epsl.2005.04.005

Rango A (1996) Spaceborne remote sensing for snow hydrology applications. Hydrol Sci J 41(4):477–494

Rango A (1997) Response of areal snow cover to climate change in a snowmelt-runoff model. Ann Glaciol 25:232–236

R-ArcticNet v 3.0 (2003) A regional, electronic, hydrographic data network for the Arctic region. http://www.r-arcticnet.sr.unh.edu/

Rigor IG, Colony RL, Martin S (2000) Variations in surface air temperature observations in the Arctic, 1979–97. J Clim 13:896–914. doi:10.1175/1520-0442(2000)013<0896:VISATO>2.0.CO;2

Rodell M, Chen J, Kato H, Famiglietti J, Nigro J, Wilson C (2006) Estimating ground water storage changes in the Mississippi river basin using GRACE. Hydrogeol J doi:10.1007/s10040-006-0103-7

Rossow WB, Schiffer RA (1999) Advances in understanding clouds from ISCCP. Bull Am Meteorol Soc 80:2261–2287. doi:10.1175/1520-0477(1999)080<2261:AIUCFI>2.0.CO;2

Serreze MC, Bromwich DH, Clark MP, Ertringer AJ, Zhang T, Lammers R (2003) Large-scale hydro-climatology of the terrestrial Arctic drainage system. J Geophys Res 107:8160. doi:10.1029/2001JD000919

Serreze MC, Barrett AP, Lo F (2005) Northern high latitude precipitation as depicted by atmospheric reanalysis and satellite retrievals. Mon Wea Rev 133(12):3407–3430. doi:10.1175/MWR3047.1

Shiklomanov IA, Lammers RB, Peterson BJ, Vorosmarty CJ (2000) The dynamics of river water inflow to the Arctic Ocean, in the freshwater budget of the Arctic Ocean. Proceedings of the NATO advanced research workshop, Tallin, Estonia, 27 April–1 May 1998, pp 281–296, Kluwer Academic Publishers, Norwell

Smith LC (1997) Satellite remote sensing of river inundation area, stage and processes: a review. Hydrol Process 11:1427–1439. doi:10.1002/(SICI)1099-1085(199708)11:10<1427::AID-HYP473>3.0.CO;2-S

Smith LC, Isacks BL, Forster RR, Bloom AL, Preuss I (1995) Estimation of discharge from braided glacial rivers using ERS 1 synthetic aperture radar: first results. Water Resour Res 31(5):1325–1329. doi:10.1029/95WR00145

Smith LC, Isacks BL, Bloom AL (1996) Estimation of discharge from three braided rivers using synthetic aperture radar satellite imagery: potential application to ungaged basins. Water Resour Res 32(7):2021–2034. doi:10.1029/96WR00752

Tapley BD, Bettadpur S, Ries JC, Thompson PF, Watkins M (2004) GRACE measurements of mass variability in the Earth system. Science 305:503–505. doi:10.1126/science.1099192

Vorosmarty CJ, Willmott CJ, Choudhury BJ, Schloss AL, Steams TK, Robeson SM et al (1996) Analyzing the discharge regime of a large tropical river through remote sensing, ground-based climatic data, and modeling. Water Resour Res 32(10):3137–3150. doi:10.1029/96WR01333

Vorosmarty CJ, Hinzman LD, Peterson BJ, Bromwich DH, Hamilton LC, Morison J et al (2001) The hydrologic cycle and its role in arctic and global environmental change: a rationale and strategy for synthesis study. Arct Res Consortium of the United States, Fairbanks, Alaska, 84 pp

Wang XL, Cho H-R (1997) Spatial-temporal structures of trend and oscillatory variabilities of precipitation over northern Eurasia. J Clim 10:2285–2298. doi:10.1175/1520-0442(1997)010<2285:STSOTA>2.0.CO;2

Yang D, Kane DL, Hinzman LD, Zhang X, Zhang T, Ye H (2002) Siberian Lena river hydrologic regime and recent change. J Geophys Res 107(D23):4694. doi:10.1029/2002JD003149

Yang D, Robinson D, Zhao Y, Estilow T, Ye B (2003) Stream flow response to seasonal snow cover extent changes in large Siberian watersheds. J Geophys Res 108(D18):4578. doi:10.1029/2002JD003149

Yang D, Zhao Y, Armstrong R, Robinson D, Brodzik M-J (2007) Streamflow response to seasonal snow cover mass changes over large Siberian watersheds. J Geophys Res 112:F02S22. doi:10.1029/2006JF000518

Ye H, Cho H, Gustafson PE (1998) The changes in Russian winter snow accumulation during 1936–83 and its spatial patterns. J Clim 11:856–863. doi:10.1175/1520-0442(1998)011<0856:TCIRWS>2.0.CO;2

Zhang T, Barry RG, Knowles K, Heginbottom JA, Brown J (1999) Statistics and characteristics of permafrost and ground-ice distribution in the Northern Hemisphere. Polar Geogr 23(2):132–154